SCIENCE CHINA
Technological Sciences

•Article•

April 2021 Vol.64 No.4: 729–744
https://doi.org/10.1007/s11431-020-1697-7

A multi-objective study on the constructal design of non-uniform heat generating disc cooled by radial- and dendritic-pattern cooling channels

CHEN Chen[1,3], YOU Jiang[1,2,4], FENG HuiJun[1,2] & CHEN LinGen[1,2*]

[1] *Institute of Thermal Science and Power Engineering, Wuhan Institute of Technology, Wuhan 430205, China;*
[2] *School of Mechanical & Electrical Engineering, Wuhan Institute of Technology, Wuhan 430205, China;*
[3] *School of Optical Information and Energy Engineering, Wuhan Institute of Technology, Wuhan 430205, China;*
[4] *College of Power Engineering, Naval University of Engineering, Wuhan 430033, China*

Received May 5, 2020; accepted July 17, 2020; published online February 4, 2021

A three-dimensional disc model with non-uniform heat generating is built. A series of cooling channels are inserted to cool this disc which is strewn in a hierarchical pattern. To reveal thermal and flow characteristics, a composite objective function comprised of the maximum temperature difference (MTD) and pumping power is constructed. The deployment pattern of cooling channels contains two cases, i.e., the radial-pattern and dendritic-pattern. By capitalizing on constructal design method together with finite element method, the diameter of radial-pattern cooling channels is optimized in the first place. Next, the diameter, angle coefficient and length coefficient of dendritic-pattern cooling channels are three degrees-of-freedom to be stepwise optimized at different heat generating conditions. Furthermore, NSGA-II algorithm is introduced into the multi-objective problem. Upon obtaining its Pareto optimal solution set, Topsis method is invoked to yield the optimal solutions under given weighted coefficients. The heat generation over the entire body and the volume ratio of cooling channels operate as the primary constraints. Based on these premises, constructal design will be stepwise performed by varying three degrees-of-freedom. The obtained results state that more heating components or devices should be installed as close to the cooling water inlet as possible. This can further reduce MTD at the same cost of pumping power, thereby improve thermal and flow performance and prolong the lifespan of devices. As optimized with two degrees-of-freedom, the MTD is reduced by 18.6% compared with the counterpart obtained from single degree-of-freedom optimization, while the pumping power is increased by 59.8%. As optimized with three degrees-of-freedom, the MTD is decreased by 6.2% compared with the counterpart from two degrees-of-freedom optimization, while the pumping power is increased by 3.0%. It is manifest that when two sub-objectives form a composite objective, the performance improvement of one sub-objective will inevitably elicit the vitiation of the alternative.

constructal law, non-uniform heat generating disc, heat convection, cooling channels, multi-objective optimization, generalized thermodynamic optimization

Citation: Chen C, You J, Feng H J, et al. A multi-objective study on the constructal design of non-uniform heat generating disc cooled by radial- and dendritic-pattern cooling channels. Sci China Tech Sci, 2021, 64: 729–744, https://doi.org/10.1007/s11431-020-1697-7

1 Introduction

Catering to the phenomenal ever-increasing demand of portable electronic products, electronic products are markedly upgrading towards high-speed, lightweight, multi-functional, low power consumption and other prospects. At the same time, their packaging structures are developing more compact, which have conceivably behaved the li-

* Corresponding author (email: lingenchen@hotmail.com; lgchenna@yahoo.com)

abilities of thinness and miniaturization. The significant advancement of integrated circuit sheds light on the evolution of advanced packaging technologies. Whereas, the roadblock arising from high demand for potent heat dissipation has turned increasingly tougher. Around recent years, the highest power of integrated circuits will exceed 360 W/cm^2, which poses severe obstacles to the efficient heat dissipation of electronic products [1]. In order to defeat the inevitable dilemma due to miniaturized electronic products along with high power density, enhanced convective heat transfer provides a viable solution as matters stand. Since Tuckerman and Pease [2] pioneered the application of micro-channels to cool an electronic chip, the micro-channel cooling technique has been made tremendous advances and gradually moves towards a market-oriented industrialization, especially in the aspect of cooling electronic products. As a result, plenty of research attentions have been riveted on the geometry optimizations of cooling channels [3], which has edified a broader lore of how micro-channels can improve the heat dissipation performance.

Constructal theory was put forward by Bejan [4,5], the gist of which could be expatiated that the structural evolution originates from providing an increasingly more accessible gateway for the "flow" that flows through its interior. It unprecedentedly puts a fresh spin on the structural design in terms of a finite size flow system. On this basis, a score of academicians have investigated various engineering problems by resorting to constructal design method in our age [6–18], e.g., heat sinks [19–23], heat source [24] solid-gas reactors [25,26], slab continuous casting [27–29], blast furnaces [30–32], converter [33], sinter cooling process [34], reheating furnace wall [35,36], hot water network [37], gas turbine blade [38], various heat exchangers [39–43], fins [44–50], vascular networks [51], dual-pressure turbine [52], and energy conversion systems [53–55]. Amongst, the constructal design of convective heat dissipation problem in the disc is a concerned aspect.

On the arena of constructal design for uniform heat generating disc, Wechsatol et al. [56] firstly utilized analytical method to research the two-dimensional steady-state "disc-point" thermo-fluid model by minimizing the total flow resistance. It was reported that the optimal flow resistance performance could be obtained by increasing the internal structural complexity of cooling pattern in the case that the shortest distance between the cooling channels remained invariant. Inspired by the research carried out in ref. [56], Lorente et al. [57] re-examined the "disc-point" heat convective problem with the minimizations of flow path length and total flow resistance, respectively. The analytical results proved that under the same geometric restraints, the optimal geometry yielded from minimizing flow path length is not much different from the counterpart yielded from minimizing total flow resistance. Wechsatol et al. [58] documented the monotonous decreasing characteristic of the maximum thermal resistance versus pumping power under the constraints of constant disc geometry and cooling channel volume. The numerical results indicated that the optimal geometry of the cooling channel obtained from the minimum total thermal resistance was radial-pattern flow structure, which was contrary to the dendritic-pattern flow structure obtained from the minimum pumping power. Reddy et al. [59] presented the thermo-fluid disc models with steady and transient states, respectively, and they showed that increasing the structural complexity of flow pattern brought benefits to the uniformity of temperature in the disc-shaped body. Besides, the decreasing trend of total thermal resistance slowed down as the internal complexity of cooling pattern increased. Revellin et al. [60] considered the influence of fluid phase change and optimized the dendritic-pattern circular flow path by means of maximizing the critical heat dissipation rate. In their research, the cooling pattern that chose radial- or dendritic-pattern deployment should be determined by the practical pumping power. Daguenet-Frick et al. [61] fed R134a into the disc strewn with radial- and dendritic-pattern cooling channels, and minimized the flow resistance by numerical method. It was shown that increasing the structure complexity of cooling pattern was not tantamount to the improvement of thermo-fluid performance. Ghaedamini et al. [62] configured the disc with recirculating micro-channels so as to procure a disc configuration with better heat transfer performance. They revealed that the realization of high heat dissipation rate required more pressure drop as cost, beyond that reducing the thickness of the disc could decrease the heat resistance to some extent. Feng et al. [63] commenced to minimize the maximum temperature difference (MTD) and re-optimized the "disc-point" convective thermal and flow problem proposed by ref. [56]. In tune with constant total pumping power, the optimal constructs of cooling channels were thus obtained by analytical method, and the radial- or dendritic-pattern arrangement of cooling channels was crucially affected by the critical disc radius. Salimpour and Menbari [64] chose the minimum total flow resistance and thermal resistance as optimization objectives and then surveyed the optimal arrangement of cooling channels. It was presented that the mass flow rate of cooling fluid behaved a great impingement on the maximum thermal resistance. On the contrary, the flow resistance was scarcely affected by the variance of mass flow rate. Apart from the abovementioned papers, many scholars put their focal points of interest on the distributions of cooling channels at various conditions of heat flux inputs [65–76].

As the practical electronic devices function commonly, the components strewn over the printed circuit board (PCB) are separately powered by the copper layers which are non-uniformly coated on the surface. On account of the diversities in the operating power and install position of individual

component, the localities with different local heat current are dispersed on the surface of PCB. As a result, the non-uniform heat generating (NUHG) phenomenon will take place in the package. In the case that the generated heat flux cannot be promptly output into the ambient, the real-time performances of the electronic devices will be inevitably compromised. So far as in this stage without any retrofits, it will incur great damage to the operating characteristics, and eventually lead to a greatly shortened lifespan of the devices. Henceforth, it merits a particular investigation of how NUHG will impinge upon the thermal and flow performance. Intended to reveal the effects of NUHG phenomenon and mend the foregoing literature gap, You et al. [77] implemented a constructal design for NUHG rectangular body which was cooled by circular channels placed in parallel pattern. They utilized alumina ceramics and water as the heat generating material and cooling fluid, respectively, afterwards verified and validated the credence of mathematical solution by experiments. Apart from riveting on heat convection problem, some academicians also made use of constructal design method to research the heat dissipation performance of heat conduction whilst the computational domain was non-uniformly heat generating [78–84]. Accordingly, Figure 1 manifestly showcases the redrawn flowchart with regard to the constructal design method based on ref. [85]. With the light of the aforementioned latest publications, constructal design method is exploited in the following procedures.

In order to study the heat dissipation performances of real electronic devices, one can regard these devices as NUHG bodies. Especially, in terms of disc-shaped electronic devices, one can insert cooling channels to tackle the high heat dissipation demand. On this basis, a three-dimensional steady-state disc model will be built to reveal the heat transfer and fluid flow characteristics. The deployment pattern of cooling channels contains two cases, i.e., the radial-pattern and dendritic-pattern. First, the diameter of radial-pattern cooling channels is optimized under different heating conditions. Next, the diameter, angle coefficient and length coefficient of dendritic-pattern cooling channels are three degrees-of-freedom to be stepwise optimized under different heat generating conditions, which is inspired by constructal design method. A composite objective function comprised of the MTD and pumping power is utilized as the optimization objective. Here, the exhaustive search method will be adopted in order to uncover the constructal design in the range of values used. Then, the multi-objective problem is further optimized by NSGA-II algorithm and on this basis its Pareto optimal solution set is yielded. Based on the Topsis multi-attribute decision method, the final solutions under specific weighted coefficients are procured by inputting the target weighted coefficients offered by the decision maker. Finally, the effects of NUHG coefficient on the geometry evolution of the pattern are analyzed.

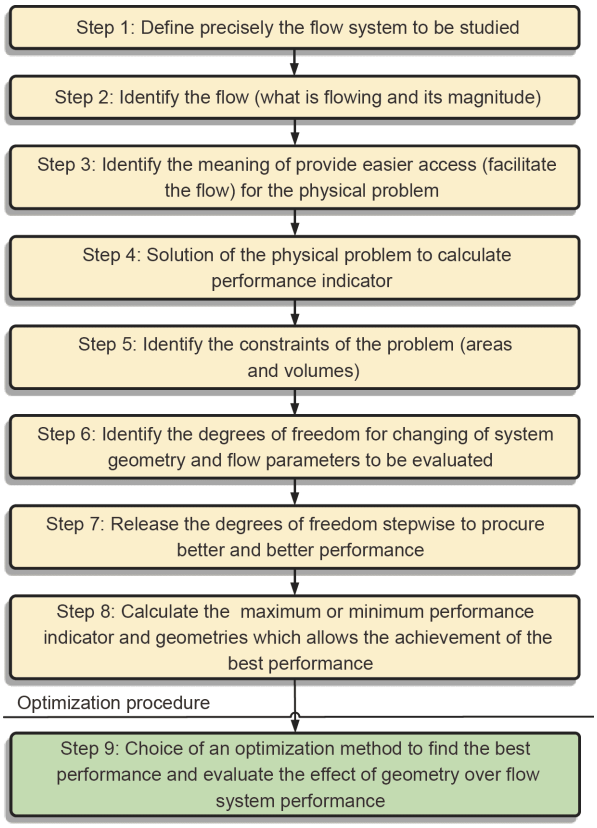

Figure 1 (Color online) Flowchart with regard to the constructal design method redrawn based on ref. [81].

2 Model establishment

2.1 Physical modeling

Normally, an electronic device can be simplified and regarded as a control body with internal heat generating as it is in steady operation. Figure 2 depicts the physical model of a disc-shaped control body. It is clear from Figure 2(a) and (b) that, r and H denote the diameter and height of the disc-shaped body, respectively. N circular cooling channels are radially arranged in the body, which are also uniformly strewn along the radial direction. Cooling fluid flows through inside so as to steer the generated heat away from the disc-shaped body. The diameter of cooling channels is d_c, and in the meantime the volumetrically heat generating coefficient in the control body is q'''. As depicted in Figure 2(b), one can notice the symmetrical characteristic of the flow pattern in the disc-shaped body, therefore, the entire disc-shaped body can be stripped into N identical unit sectors. To this end, the unit body that featuring volume v_{el} and apex angle $2\theta_0$ can be particularly isolated as the research geometry. Furthermore, for the brevity of numerical calculation, the model shown in Figure 3 is finally ascertained to be the computational domain solved by the finite element method. Under the hypothesis of the invariable volume of disc-shaped body, both the height $H/2$ and radius r vary with

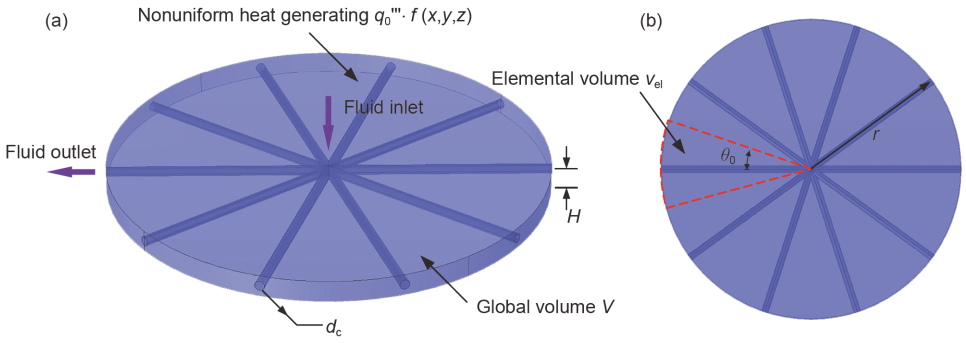

Figure 2 (Color online) Thermo-fluid model for a NUHG disc-shaped body. (a) Stereo view; (b) top view.

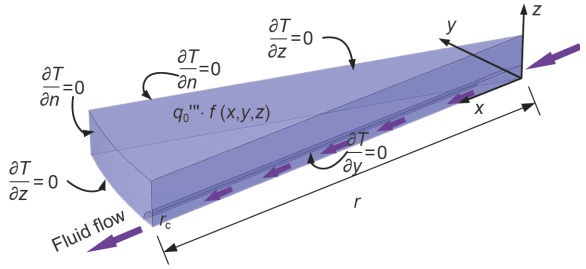

Figure 3 (Color online) Computation domain and relative boundary conditions.

Table 1 Geometrical parameters of a NUHG disc-shaped body

Parameters	Expressions	Notices
V	$\pi r^2\cdot H$	Constant, volume restriction
N	–	Independent variable
v_{el}	$\pi r^2\cdot H/N$	Dependent variable
d_c	–	Independent variable
H	$(d_c/r)^2\cdot r\cdot N/(4\cdot\phi)$	Dependent variable, ϕ denotes volume ratio restriction
r	$\sqrt{V/\pi H}$	Dependent variable

the number of cooling channels. Table 1 lists the geometric parameters and the mutual relationships among them. Given the unit body, the heat generated inside the unit sector is first conveyed to the interface of cooling channel by heat conduction in the heat generating substrate with thermal conductivity k_s. In the next, the heat is exported away from the unit sector through heat convection process among the cooling fluid and the interface. From Table 1, the cross-section of circular cooling channel is $\pi d_c^{\,2}/4$, and its volume proportion to the unit sector is defined as the volume ratio of cooling channel to unit sector, which can be computed by

$$\phi = v_{ch}/v_{el} = (d_c/r)^2\cdot r\cdot N/(4\cdot H), \tag{1}$$

and the volume of unit sector is

$$v_{el}=\pi H r^2/N. \tag{2}$$

The total heat generating rate in the entire disc-shaped body is fixed, that is

$$\dot{Q} = V\cdot q_0''' = \int_V q'''\,\mathrm{d}v, \tag{3}$$

where q_0''' is denominated as the NUHG constant. In this precondition, eq. (3) serves as a general heat generating constraint in the following calculations.

Pertinent to the background of industrial application, on the notice of widely differing power consumption and install position of individual component, the heat generated over the genuine electronic devices is commonly non-uniform distributed. Intended to study the influence of NUHG on the thermal and flow characteristics, the heat generating rate is presumed to linearly decrease along the radial direction. In this case, q''' is equal to $q_0'''\cdot(1+0.1p-0.15p\cdot\bar{r})$ according to refs. [77,86], among which $\bar{r}$ is nondimensionalized as $(x^2+y^2)^{1/2}/r$ (x and y denote the spatial location in the xy plane) and p denotes the NUHG coefficient. It is obvious that various values of p can dictate different cases of heat generating. Upon completing the non-uniform heat source, one can burrow into the mechanism of how NUHG will impinge upon the optimal flow pattern to cooling a disc-shaped body both qualitatively and quantitatively.

2.2 Numerical modeling

Alumina ceramics (Al_2O_3) are characterized by their fine thermal conductivity, robust heat resistance as well as eligible mechanical strength. In this regard, alumina ceramics have been widely employed to fabricate the substrate for integrated circuit board. This paper selects the high-purity alumina ceramics as the heat generating material and chooses water as the cooling fluid. On this basis, the generated heat is exported out of the disc-shaped body by the cooling water that flowing through the radially distributed cooling path. In order to complete the definitions of respective materials, Table 2 lists the thermal properties of alumina ceramics and cooling water.

In terms of the three-dimensional steady-state model of a

Table 2 Thermo-physical properties

Materials	Thermo-physical properties	Values
Alumina ceramics (Solid region)	Density (kg/m^3)	3900
	Specific heat (J/(kg K))	900
	Thermal conductivity (W/(m K))	27
Water (Cooling fluid)	Density (kg/m^3)	998
	Specific heat (J/(kg K))	4180
	Thermal conductivity (W/(m K))	0.61042
	Dynamic viscosity (Pa s)	8.0183×10^{-4}

NUHG disc as presented in Figure 3, the following simplified assumptions are enumerated here.

(1) The solution is carried out in the case of Re<2300 (Reynolds number), where both the heat transfer and fluid flow are in steady state. Moreover, the flow is considered laminar and fully developed.

(2) The fluid flows without any phase change and in the meantime is incompressible.

(3) The thermo-physical properties of heat generating material and cooling fluid are substantially immutable with the temperature variance. The uniform and isotropic thermal conductivity material is adopted in the solid part.

(4) The wall which environs the cooling fluid is applied by no-slip boundary condition.

(5) The heat dissipation owing to viscous dissipation is disregarded. Besides, the effect of gravity is also not taken into account.

In line with the foregoing presumptions, the governing equations to depict the convective heat transfer problems can be yielded. The mass, momentum and energy conservation equations describing the thermal and flow characteristics in the cooling channels are given as

$$\frac{\partial}{\partial X_i}(\rho_{\mathrm{f}}\cdot u_i)=0, \tag{4}$$

$$\frac{\partial}{\partial X_i}(\rho_{\mathrm{f}}u_iu_j)=-\frac{\partial P}{\partial X_j}+\frac{\partial}{\partial X_i}\left(\mu_{\mathrm{f}}\frac{\partial u_j}{\partial X_i}\right), \tag{5}$$

$$\frac{\partial}{\partial X_i}\left(\rho_{\mathrm{f}}u_ic_{\mathrm{p,f}}T\right)=\frac{\partial}{\partial X_i}\left(k_{\mathrm{f}}\frac{\partial T}{\partial X_i}\right), \tag{6}$$

where X denotes the spatial dimension, u denotes the velocity component, and the subscripts i and j (=1, 2, 3) dictate the three axis directions, respectively; μ_{f} denotes the dynamic viscosity, ρ_{f} denotes the density, $c_{\mathrm{p,f}}$ denotes the heat capacity, k_{f} denotes the conductivity, and the subscript f dictates the thermo-physical properties of cooling fluid; P denotes the pressure distribution in the cooling channel; T denotes the temperature distribution in the computational domain.

In the alumina ceramics with NUHG, the differential equation to describe the three-dimensional steady-state heat conduction is given as

$$\frac{\partial}{\partial X_i}\left(k_{\mathrm{s}}\frac{\partial T}{\partial X_i}\right)+q_0'''(1+0.1p-0.15p\cdot\vec{r})=0, \tag{7}$$

where k_{s} denotes the conductivity of alumina ceramics.

In addition to the listed governing equations, Table 3 further gives the pertinent boundary conditions which are requisite to integratedly solve eqs. (4)–(7).

(1) Cooling fluid inlet: The mass flow rate of cooling fluid flowing into the unit sector is $\dot{m}$, at which the temperature is hold at 300 K coming from a thermostatic water cabinet. As to ascertain that the fluid flow is always in laminar state, the mass flow rate varies between 2.0×10^{-4} and 1.8×10^{-3} kg/s after numerical verification. In this paper, the numerical optimization is carried out under several sets of mass flow rate.

(2) Cooling fluid outlet: The outlet is loaded with pressure outlet condition, which features a constant value of P_{put} =0 Pa. In the cooling channel, subtracting the pressure of inlet from that of outlet can yield the pressure drop.

(3) Wall: The outskirts of alumina ceramics are entirely adiabatic, besides that the solid and fluid interface is in strict concord with the continuity equations of temperature and heat flow density.

By solving eqs. (4)–(7) along with corresponding boundary conditions, one can obtain the temperature distribution in the unit sector and the pressure drop features in the cooling channel. Henceforth, the MTD within the unit sector can be obtained by

$$\Delta T=T_{\max}-T_{\min}, \tag{8}$$

where $T_{\max}$ and $T_{\min}$ denote the temperatures of the hotspot and cooling water inlet, respectively.

The pressure drop loss caused by water flowing in a single cooling channel is derived as

$$\Delta P=P_{\mathrm{in}}-P_{\mathrm{out}}. \tag{9}$$

One can further yield the pumping power required in the whole disc-shaped body:

$$\dot{W}=\dot{M}\Delta P/\rho_{\mathrm{f}}=N\cdot\dot{m}\Delta P/\rho_{\mathrm{f}}, \tag{10}$$

where $\dot{M}$ denotes the total mass flow rate of cooling water that flowing through the disc-shaped body, i.e., $\dot{M}=N\cdot\dot{m}$.

Table 3 Related boundary conditions[a)]

Positions	Boundary conditions for fluid flow and heat transfer
Inlet	Mass flow rate $\dot{m}$ (2.0×10^{-4}–1.8×10^{-3} kg/s) Temperature 300 K
Outlet	Pressure outlet $P_{\mathrm{out}}=0$
Walls	No-slip wall, $\frac{\partial T}{\partial n}=0$
Interface	No-slip wall, $k_{\mathrm{f}}\frac{\partial T_{\mathrm{f}}}{\partial n}=k_{\mathrm{s}}\frac{\partial T_{\mathrm{s}}}{\partial n}$

a) n denotes the normal direction of the relative wall.

As mentioned above, both the MTD and pumping power are worthy of full attention. Backed by practical industrial applications, one sub-objective cannot be simply exerted while the alternative is left behind. A composite objective function comprised of the MTD and pumping power is built up herein, so as to evaluate the trade-off effect of enhanced convection for a NUHG disc-shaped body. Its physical significance can be regarded as two different cases as follows. On the one hand, one can relish the smaller hot spot temperature as the same amount of pumping power is consumed. On the other hand, one can also relish the smaller pumping power as the hot spot temperature is the same. Thus, it is evident that the thermal and flow performance is superior in the case of a smaller composite function value. The composite objective function F_{TW} can be defined according to ref. [77], that is

$$F_{\mathrm{TW}} = \lambda_0 \frac{\Delta T}{\Delta T_{\mathrm{int}}} + (1-\lambda_0)\frac{\dot{W}}{\dot{W}_{\mathrm{int}}}, \tag{11}$$

where λ_0 denotes the weighted coefficient, which varies between 0 and 1 and can be determined according to the variances in the importance of each sub-objective and the demands for tangible industrial applications.

The conjugate thermal and flow problem of a NUHG disc can be depicted as the following optimization problems.

(1) Objective function: The composite objective function F_{TW} which bridges a collaborative trade-off between the MTD and pumping power, i.e.,

$$\text{Minimize } F_{\mathrm{TW}}. \tag{12}$$

(2) Design variables: The dimensionless diameter ($\tilde{d} = d_c/r$) of cooling channel.

(3) Design constraints: The volume of the entire disc-shaped body is constant along with that the volume ratio of cooling channels is invariant. Because of the constant volumetric heat generating coefficient q_0''', the general heat generating rate also stays unchanged. These constraints are given as

$$\iiint_V \mathrm{d}v = \text{Constant}, \tag{13}$$

$$\phi = v_{\mathrm{ch}}/v_{\mathrm{el}} = \text{Constant}, \tag{14}$$

$$\iiint_V q_0''' \cdot f(x,y,z)\mathrm{d}v = \text{Constant}. \tag{15}$$

3 Constructal design based on composite objective function

With the exertion of the finite element method, COMSOL Multiphysics is resorted to numerically solve eqs. (4)–(7) abided by corresponding boundary constraints. For brevity, Figure 4 presents the detailed and step-by-step scheme for how to implement the constructal design in terms of enhanced convective problem of a NUHG disc. The explicit solving procedures mainly consist of these as follows.

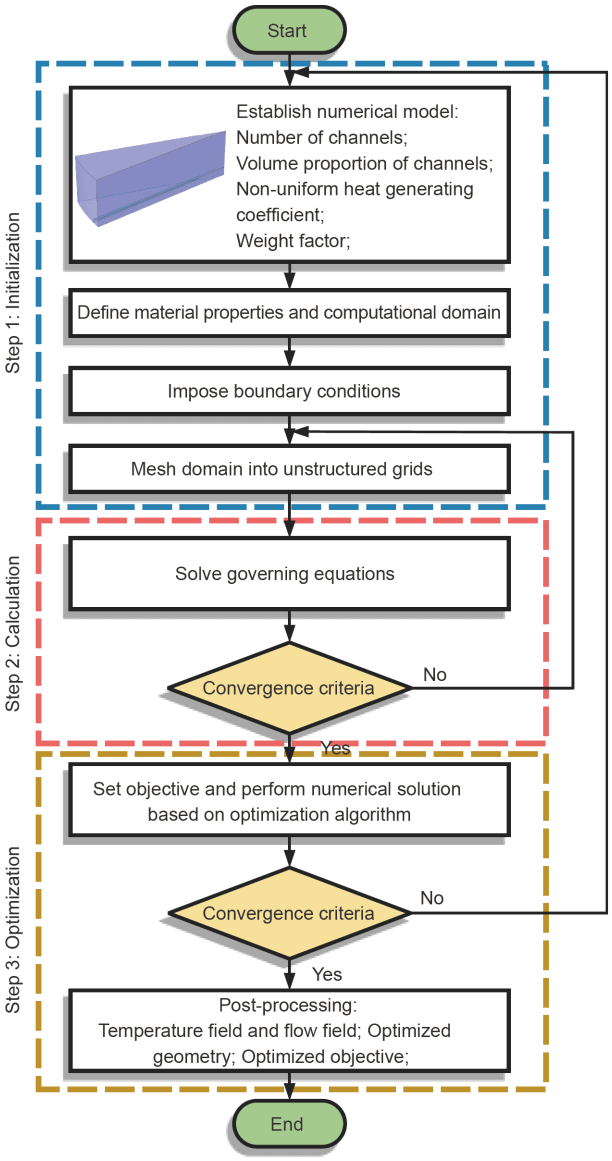

Figure 4 (Color online) Flow diagram of numerical solution for enhanced convective problem in a NUHG disc-shaped body.

(1) Define the material properties, computational domain as well as respective boundary conditions. In the meantime, initialize the original geometric parameters for the unit sector.

(2) Proceed with the unstructured meshing. Yield the temperature distribution and fluid flow field by solving the foregoing governing equations.

(3) Compute the MTD and pumping power as the two sub-objectives.

(4) Estimate the criteria of governing equations whether to converge or not. If not, then repeatedly resume step *i* until the convergence criteria are satisfied.

(5) Choose exhaustible search algorithm to obtain the

optimal solution of constructal design, and determine whether the composite objective function is minimized. If not, then resume step *i*.

(6) Post-process and analyze.

3.1 Radial-pattern disc

During meshing process, tetrahedral unstructured grid is employed to mesh both the solid region and fluid domain. Apropos of that the solid-fluid interface behaves a severe impact on the heat convection, as a result, appropriate refinement of mesh for this interface is added. Before proceeding any further, the grid independence is corroborated in order to eliminate the influence of the grid precision on the numerical results.

In the case that the unit sectors N=10 in entire disc-shaped body, the NUHG coefficient p=0 (viz. the alumina ceramics are uniformly heat generating), the volume ratio ϕ=0.05, the diameter d_c=3 mm of cooling channels and the mass flow rate $\dot{M}=8.0\times10^{-4}$ kg/s of cooling water in single unit sector, the grid precisions are separately set as coarse, regular, fine, finer and ultra-fine ones. The obtained numerical results under different mesh precisions are evaluated through a contrastive analysis. Table 4 lists the grid numbers of five sets, in which the correlative MTD and pumping power for each case are also given. As listed in Table 4, as the grid number is 135004 regarding the computational domain only, the MTD and pumping power are 46.05 K and 3.72×10^{-4} W, respectively. If proceed with refinement to the grid number of 275528, the counterparts respectively varies 0.13% and 1.3%, which is leading to a comprehensive 0.7% variance for the composite objective function. Taking account the time cost and required accuracy, the fourth set of grid precision is applied as the meshing template in this paper. Beyond that, the continuity and energy convergence criteria are restrained as 1×10^{-4} and 1×10^{-6}, respectively. Figure 5 shows the grid model with an unstructured grid number of 135004. It can be seen from eq. (11) that, prior to the constructal design of NUHG disc, the initial performance indexes (i.e., ΔT_{int} and $\dot{W}_{\text{int}}$) should also be given. The initial geometric dimensions plus the performance indexes are listed in Table 5.

To deal with the verification of numerical results, it is veritable to compare the results yielded from the aforementioned numerical solution with the counterparts yielded from analytical solution in ref. [63]. For $\tilde{d}=0.023$, the temperature difference between the cooling water inlet and outlet is 10.0 K based on numerical solution, which features a 16.3% variance compared with the counterpart based on analytical solution. In addition, the pumping power is 4.1×10^{-4} W based on numerical solution, which features a 14.5% variance compared with the counterpart based on analytical solution. Therefore, it is vindicated that the proposed numerical solution is authentic with regard to ref. [63].

Figure 6 presents the variations of the MTD and pumping power in the disc-shaped body versus the dimensionless diameter $\tilde{d}$ of the cooling channels. As shown in Figure 6, the MTD behaves an extreme value with the increase of dimensionless diameter, while the pumping power decreases monotonously. This is due to the appendant effect that the disc-shaped body is thinner as $\tilde{d}$ is smaller. On the one hand, because the radial-pattern disc is rather flat, the zone far away from the cooling channels is not effectively cooled, which leads to a high temperature difference among the heat generating body. On the other hand, the flow resistance along the cooling channels shoots up in the case of smaller $\tilde{d}$, as a result the pressure drop loss severely increases. Referred to eq. (10), the pumping power is linear with the pressure drop loss, thus $\dot{W}$ is larger at smaller $\tilde{d}$. When $\tilde{d}$ increases gradually, the height of the disc increases likewise. At the same time, the heat generated in the region far away from the cooling path can also be conveyed by the cooling water. Thus the MTD can be reduced by this means, and obviously the minimum value can be obtained at a proper condition. With the further increase of $\tilde{d}$, the structure of radial-pattern disc morphs slenderer and longer. This results in that the zone far away from the internal cooling path along the z direction cannot be effectively cooled, thus the MTD increases again. Normally, the engineering designers always relish to use the least cost (the pumping power is the minimum) to procure the largest profit (the MTD is the minimum). Whereas, as revealed in Figure 6, the MTD and pumping power are two contradictory sub-objectives that forms a game against each other. It is never going to happen that achieving the minimum of one sub-objective at the same time without causing the deterioration of the alternative.

Figure 7 presents the variation of the composite objective

Table 4 Grid independence corroboration[a)]

Precision	Coarse	Regular	Fine	Finer	Ultra-fine
Grid numbers	34553	61461	92832	135004 (*)	275528
ΔT (K)	45.88	45.94	46.01	46.05	46.11
$\dot{W}$ (W)	3.43×10^{-4}	3.49×10^{-4}	3.68×10^{-4}	3.72×10^{-4}	3.77×10^{-4}
F_{TW}	0.9592	0.9679	0.9942	1	1.007

a) * presents that the MTD and pumping power are selected as the initial values for numerical solution as the number of grids is 135004.

Figure 5 Grid model of computational domain.

Table 5 Initial geometrical parameters and performance indexes

Category	Parameters	Initial values
Geometrical parameters	V (m^3)	1.5×10^{-4}
	N	10
	H (m)	0.00424
	r (m)	0.1061
	V_{el} (m^3)	1.5×10^{-5}
	d_c (m)	0.003
	ϕ	0.05
Performance indicators	$\dot{Q}$ (W)	285
	$\dot{m}$ (kg/s)	8.0×10^{-4}
	ΔT (K)	46.05
	$\dot{W}$ (W)	3.72×10^{-4}

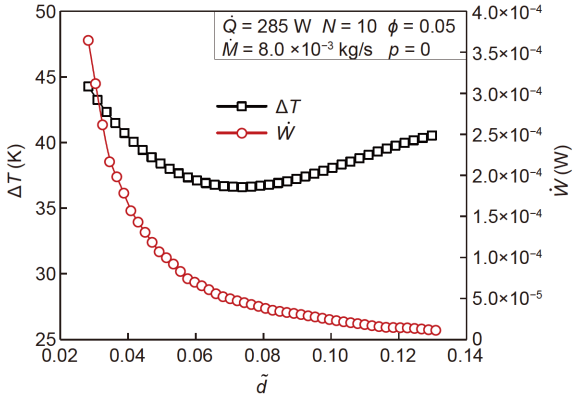

Figure 6 (Color online) Variations of ΔT and $\dot{W}$ versus $\tilde{d}$.

function F_{TW} versus the dimensionless diameter $\tilde{d}$ for different values of NUHG coefficient p. As shown in Figure 7, F_{TW} decreases first and then increases gradually as $\tilde{d}$ increases. It is clear that, under different conditions of heat generating, a minimum value ($F_{TW,m}$) of F_{TW} can be reached when $\tilde{d} = \tilde{d}_{opt}$. Note that in the case of p=9, F_{TW} is minimized to be 0.40 as $\tilde{d}_{opt}$ is equal to 0.10. As a result, the MTD (ΔT) and pumping power ($\dot{W}$) are 33.8 K and 2.29×10^{-5} W, respectively. By comparing the thermal and flow performances of initial unit sector in Table 5, ΔT and $\dot{W}$ are decreased by 26.6% and 38.4%, respectively, which coherently leads to

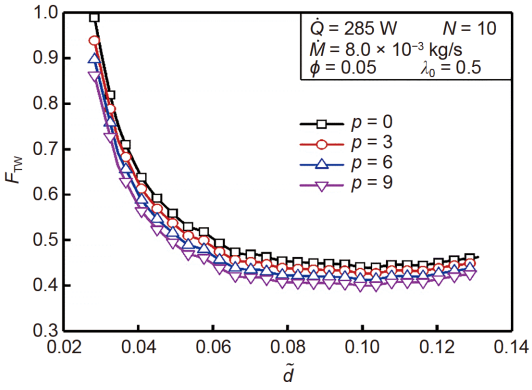

Figure 7 (Color online) Variation of F_{TW} versus $\tilde{d}$ for different values of p.

60.2% reduction in F_{TW}. It is indicated that the optimal trade-off between the MTD and pumping power can be bridged by rational selection of the diameter of cooling channels, which is capable of improving the overall thermal and flow performance. Additionally, one can notice that F_{TW} features a monotonous decrease trend against the increase of p. Besides, the optimal $\tilde{d}$ ($\tilde{d}_{opt}$) scarcely changes as p increases. The heat generating near the cooling water inlet is relatively larger. As a result, more heat is expelled by the cooling water out of the NUHG disc, and the hot spot temperature turns to decline. The composite objective function F_{TW} is decreased and the overall thermal and flow performance is elevated. It is implied that more heating components or devices should as far as possible be installed near the inlet, which can further decline the hot spot temperature in the disc-shaped body in the premise of the same pumping power. It improves the real-time operating performance and prolongs the service lifespan. In coherence with the aforementioned calculating parameters, Figure 8 presents the temperature contours of the

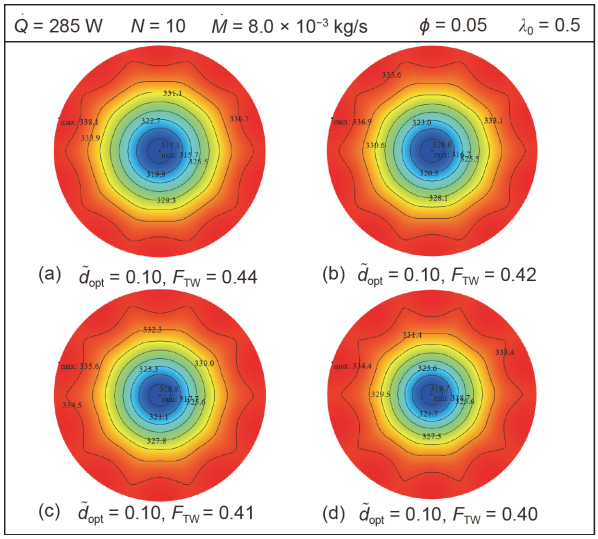

Figure 8 (Color online) Temperature contours of the optimal NUHG disc-shaped body. (a) p=0; (b) p=3; (c) p=6; (d) p=9.

optimal disc-shaped heat generating bodies at the conditions of p=0, 3, 6 and 9, respectively. It is obvious that the hot spot temperature inside the disc decreases as the NUHG coefficient increases.

Figure 9 presents the variation of F_{TW} versus $\tilde{d}$ for different values of volume ratio ϕ at p=9. For the given NUHG condition and ϕ, F_{TW} first decreases and then increases as $\tilde{d}$ increases. Besides, the minimum value ($F_{TW,m}$) of F_{TW} can be further reduced by increasing ϕ. Besides, the optimal $\tilde{d}$ ($\tilde{d}_{opt}$) gradually increases as ϕ increases, that is, the diameter of cooling channels morphs larger while the structure of disc grows slenderer in this regard. As shown in Figure 9, as the volume ratio increases from 0.03 to 0.05, the composite objective function goes down from 0.46 to 0.40, which is lowered by 13.0%. As a result, one can elevate the overall thermal and flow performance by increasing the volume ratio of the cooling channels.

Figure 10 presents the variation of F_{TW} versus $\tilde{d}$ for different values of N at p=9. As the number N of unit sectors increases from 10 to 15, $F_{TW,m}$ is decreased by 14.0%. Besides, $F_{TW,m}$ is further decreased by 8.13% as N increases from 15 to 20 according to Figure 10. In line with eq. (10), it is manifest that the pumping power that consumed to sustain fluid flow increases if the number of unit sectors increases. On the opposite side, the composite objective function shows a decreasing trend, which dictates that the benefit brought by the decrease of hot spot temperature infallibly outperforms the cost brought by the increase of pumping power. Therefore, it is implied that the improvement of overall thermal and flow performance can profit from increasing the number of cooling channels strewn in the disc-shaped body.

To further explain the variation of the composite objective function with the number of unit sectors, Figure 11 presents the influences of the number of unit sectors on the characteristics of the MTD and pumping power versus the dimensionless diameter. It can be seen from Figure 11 that, when the number of unit sectors increases, the MTD first changes slowly and then increases sharply, while the pumping power behaves differently. The pumping power firstly features a rapid decrease and then a slow decrease. Under the combined effect, there exists an extreme value of the composite objective function, so that the MTD and pumping power can finally match an optimal trade-off. From Figures 10 and 11, for possible industrial applications, the engineering designers need to equitably determine the number of cooling channels strewn in the NUHG disc in order to obtain the optimal overall thermo-fluid performance.

Figure 12 presents the variation of F_{TW} versus $\tilde{d}$ for different values of mass flow rate $\dot{M}$ at p=9. As shown in Figure 12, as $\tilde{d}$ varies between 0.028 and $\tilde{d}_{opt}$, F_{TW} increases with the increase of $\dot{M}$. This can be illuminated as: increasing the mass flow rate through the entire flow pattern, on the one hand, can ensure more cooling water to participate in the convective heat transfer and convey away more heat; on the other hand, it can also lead to the steep increasing of pumping power. The final result is the deterioration of the overall thermal and flow performance. Apart from this, one can also note that $F_{TW,m}$ gradually decreases with the increase

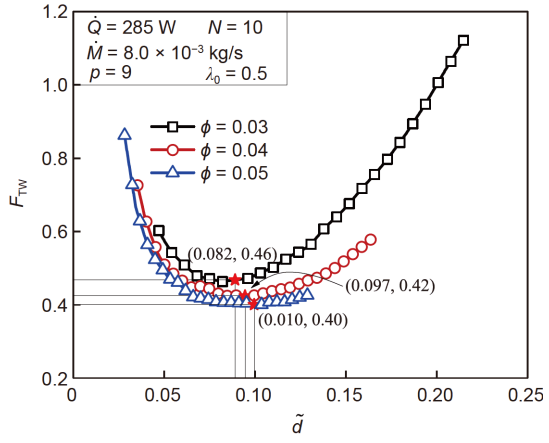

Figure 9 (Color online) Variation of F_{TW} versus $\tilde{d}$ for different values of ϕ.

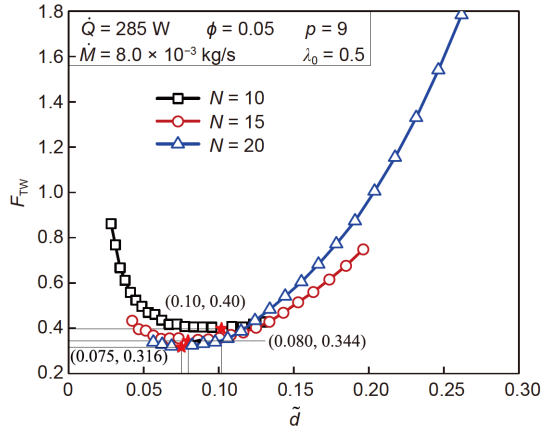

Figure 10 (Color online) Variation of F_{TW} versus $\tilde{d}$ for different values of N.

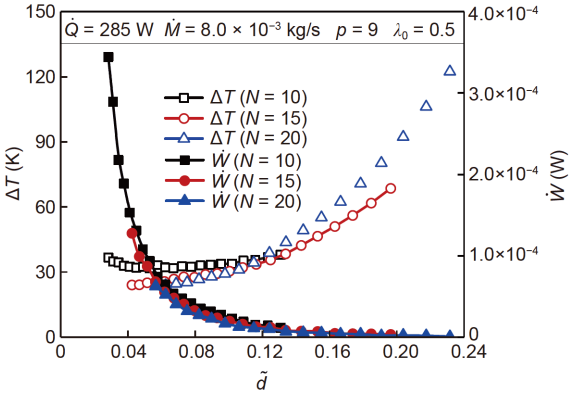

Figure 11 (Color online) Variations of ΔT and $\dot{W}$ versus $\tilde{d}$ for different values of N.

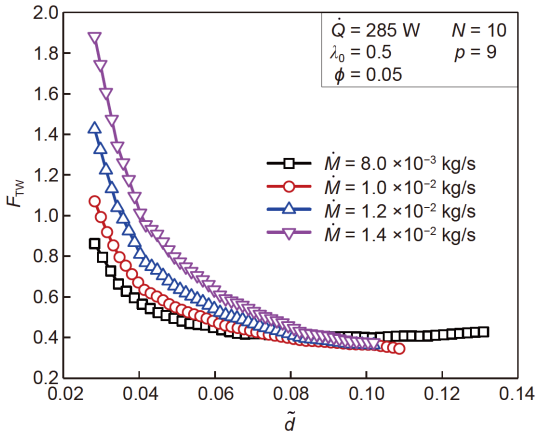

Figure 12 (Color online) Variation of F_{TW} versus $\tilde{d}$ for different values of $\dot{m}$.

of $\dot{M}$. From the above analyses, it can also be found that the engineering designers should not baselessly increase the mass flow rate attempting to elevate the thermal and flow performance, which on the contrary should be rationally selected according to practical situation.

Figure 13 presents the variation of F_{TW} versus $\tilde{d}$ for different values of λ_0 at p=9. As can be seen from Figure 13, as λ_0 increases, the optimal dimensionless diameter $\tilde{d}_{opt}$ decreases while F_{TW} gradually increases; that is, the overall thermal and flow performance is compromised to this end. On the basis of eq. (11), the increasing of weighted coefficient means that the potent demand for reducing the MTD is prior to that for reducing the pumping power. The specific value of weighted coefficient included in the composite objective function should be accordingly determined to obtain a potential trade-off between heat transfer and fluid flow.

3.2 Dendritic-pattern disc

To further improve the overall thermal and flow performance

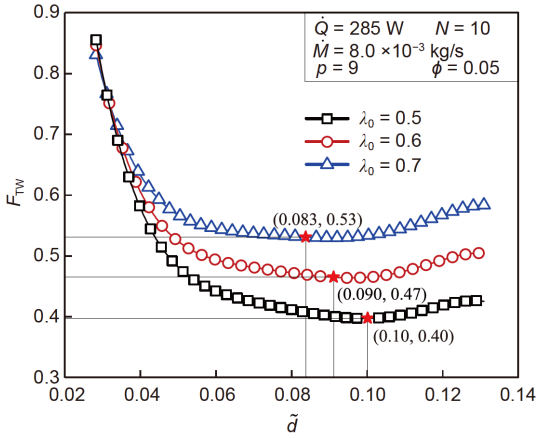

Figure 13 (Color online) Variation of F_{TW} versus $\tilde{d}$ for different values of λ_0.

of a NUHG disc, the disc model cooled by dendritic-pattern channels is established, as shown in Figure 14. The unit sector that constitutes the NUHG body of the radial-pattern disc is fabricated into a dendritic-pattern disc at the periphery. The arrangement pattern adopted in this paper is elaborated as follows: stem cooling channels (diameter d_c) are equidistantly dispersed along the circle, which outwardly extends from the center with a length of $\alpha \cdot r$ (α stands for the length coefficient). Then, each stem cooling channel is conjoint with two branch cooling channels (diameter d_c and angle $2\theta_0 = 2\beta \cdot \arctan[r \cdot \sin\theta_1 / (r \cdot \cos\theta_1 - \alpha r)]$). These branches are attached to the periphery (β denotes the angle coefficient). As mentioned above, the entire dendritic-pattern disc contains N stem cooling channels and $2N$ branch cooling channels. The stem and branch cooling channels play the roles as the bough and limb, respectively. That is, the cooling water first flows through the confluent stems and then into the tributary branches. As depicted in Figure 14(b), the apex angle of each unit sector striped from the dendritic-pattern disc is $2\theta_1$, which includes a bough and two limbs. On this basis, eqs. (4)–(7) and the corresponding boundary conditions are numerically solved by invoking the software of COMSOL Multiphysics. This optimization problem contains

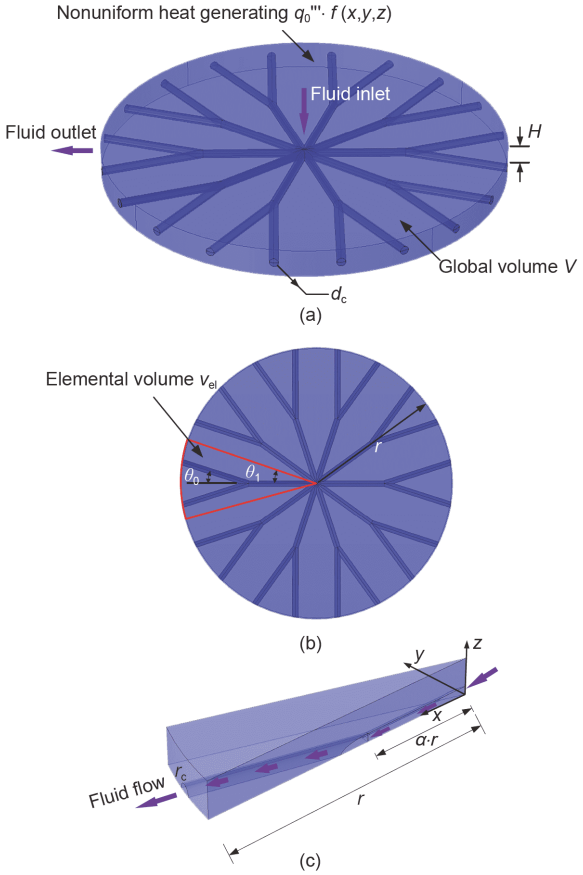

Figure 14 (Color online) Thermo-fluid model for a NUHG dendritic-pattern disc. (a) Stereo view; (b) top view; (c) computation domain.

three design variables: The dimensionless diameter $\tilde{d}$ of cooling channels, the length coefficient α and the angle coefficient β. In this section, these three variables are free to morph so as to carry out constructal design of the dendritic-pattern disc under different heat generating conditions for the thermal and flow problem as Figure 15 indicated.

Figure 16 presents the three-dimensional diagram of F_{TW} versus $\tilde{d}$ and β with α=0.5 and λ_0=0.5. As shown in Figure 16, the composite objective function obtains the quadratic minimum $F_{TW,mm}$=0.348 in the case of $\tilde{d}_{opt}$=0.074 and β_{opt}=0.73. Compared with the performance indexes of the unit with initial design listed in Table 5, ΔT and $\dot{W}$ are decreased by 42.3% and 90.2%, respectively. As a result, F_{TW} is reduced by 65.2%. From Figures 7 and 16, one can note that as the dendritic-pattern disc is quadratically optimized, the composite objective function $F_{TW,mm}$ slumps by 40.0% compared with the counterpart $F_{TW,m}$ obtained for single degree-of-freedom optimization in Sect. 3.1. It can be concluded that the superior overall thermal and flow performance can be achieved by logically selecting the dimensionless diameter of cooling channels and angle coefficient in the premise of given length coefficient.

Table 6 further lists the effects of p on the optimal geometries and performance indexes of the dendritic-pattern disc. As shown in Table 6, one can see that the optimal $\tilde{d}_{opt}$ gradually decreases as p increases, while the optimal β_{opt} first decreases and then increases and last decreases as p increases. In addition, it is manifest that as the NUHG coefficient increases from 0 to 9, more heat is generated near the cooling water inlet. Under this condition, ΔT is decreased by 13.8%, while $\dot{W}$ is increased by 37.6%. Owing to that the increase of pumping power is relatively smaller compared with the reference value of pumping power (see Table 5), it eventually reduces $F_{TW,mm}$ by 8.9%. This explicitly shows that the heat generation component should as far as possible be situated near the cooling water inlet. Although the pumping power required for cooling the dendritic-pattern disc increases to a certain extent, the hot spot temperature in the disc keeps decreasing. Thus, it is proven that increasing the NUHG coefficient is contributive to improving the overall thermal and flow performance of enhanced convection.

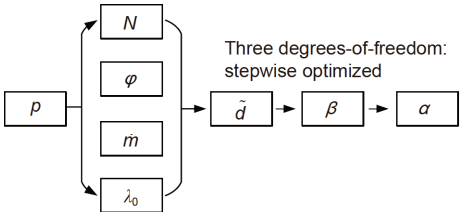

Figure 15 Flowchart of performed study with exhaustive search technique.

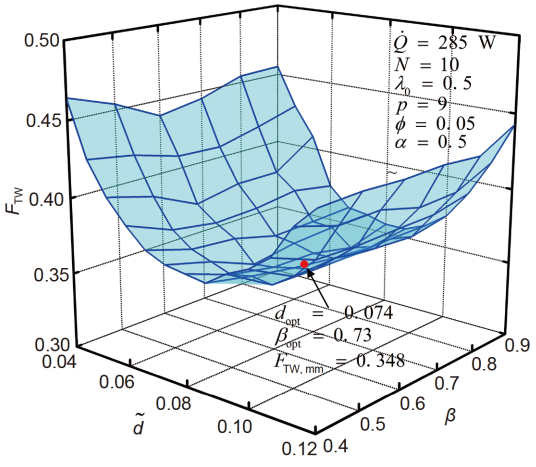

Figure 16 (Color online) Three-dimensional diagram of F_{TW} versus $\tilde{d}$ and β.

Table 6 Var iations of $\tilde{d}_{opt}$, β_{opt}, ΔT, $\dot{W}$ and $F_{TW,mm}$ for different cases of p

p	$\tilde{d}_{opt}$	β_{opt}	ΔT (K)	$\dot{W}$ (W)	$F_{TW,mm}$
0	0.0809	0.787	31.9	2.66×10^{-5}	0.382
3	0.0808	0.720	30.7	2.77×10^{-5}	0.371
6	0.0755	0.804	29.654	3.42×10^{-5}	0.358
9	0.0740	0.726	27.5	3.66×10^{-5}	0.348

Figure 17 presents the variation of the composite objective function F_{TW} versus length coefficient α at $\tilde{d}$=0.074 and β=0.73. It can be seen from Figure 17 that F_{TW} features a minimum value in the case of a proper α. This can be explained as follows: on the one hand, as α is extremely small, the stem cooling channels turn out to be rather smaller compared with the branch cooling channels, and it can be approximately regarded that the dendritic-pattern disc degenerated into a radial-pattern disc consisting of $2N$ unit sectors. Although the entire heat generating disc is cooled thoroughly, it will court the upsurge of pumping power

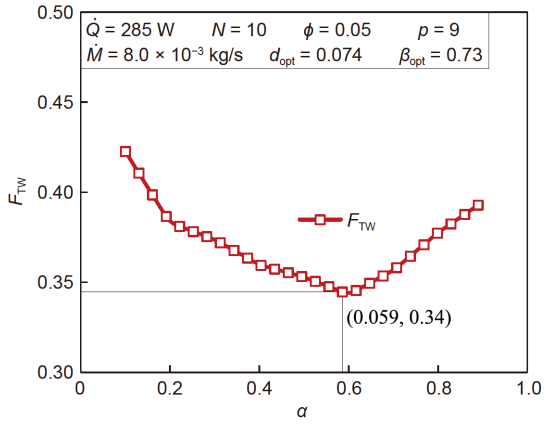

Figure 17 (Color online) Variation of F_{TW} versus α at $\tilde{d}$=0.074 and β=0.73.

(seeing eq. (10)) and behaves a poor overall thermo-fluid performance. On the other hand, as α is extremely large, the branch cooling channels morph rather shorter than the stem cooling channels, which means that in this case the dendritic-pattern disc can be assumed to degenerate into a radial-pattern disc consisting of N unit sectors. Although the pumping power is manifestly reduced, the heat generating disc is not well cooled and thus the overall thermal and flow performance is not promising. The numerical results indicate that there exists an extreme value of F_{TW} when α varies. That is, the optimal compromise between the MTD and pumping power can be attained by choosing a sound value of α.

4 Multi-objective optimization based on NSGA-II

In the above section, a composite objective function is constructed by exerting the linear weighted method, which thus transforms the multi-objective optimization problem (MOOP) into a single objective optimization problem. By taking advantage of the mature single objective optimization algorithm, the optimal solution under a given weighted coefficient is obtained. However, having noticed of the contradictory characteristics among the most of sub-objectives, it is impossible to manage an optimal solution in reality so that all the sub-objectives can behave the optimal performance at the same time. The only path is to compromise and coordinate the trade-offs among the sub-objectives, as a result the common solution of MOOP is formed by a set of non-inferior solutions, namely Pareto optimal solution set. In this section, the non-dominated sorting genetic algorithm (NSGA-II) will be utilized to probe for the optimal matchings, which is associated with elite strategy to realize the same level fast sorting. Figure 18 elaborates the flow diagram of NSGA-II in detail. As shown in Figure 18, if given that the generation excesses the upper preset limit, the optimization procedure will break up to produce the optimal Pareto solution set. In the state of the art, to its credit of potent computational efficiency, NSGA-II has aroused much attention and interest in many engineering optimization fields, and furthermore already becomes one of the mainstream solutions of MOOP [87–90].

The dendritic-pattern disc with NUHG features three degrees-of-freedom, that is the dimensionless diameter $\tilde{d}$ of cooling channels, the length coefficient α and the angle coefficient β. Herein, these three design variables are free to morph so as to yield a better thermal and flow performance. Upon choosing the optimization parameters, in order to achieve reliable convergence and global seeking of the optimization process, the following constraints are imposed on the design variables as

$$\begin{cases} 0.04 \le \tilde{d} \le 0.12, \\ 0.1 \le \alpha \le 0.9, \\ 0.1 \le \beta \le 0.9. \end{cases} \tag{16}$$

The two optimization objectives (f_1 and f_2) are the MTD (ΔT) in the dendritic-pattern disc and the pumping power ($\dot{W}$) needed to sustain enhanced convection, namely

$$\begin{cases} f_1: \ \Delta T = T_{\max} - T_{\min}, \\ f_2: \ \dot{W} = \dot{M} \Delta P / \rho_{\mathrm{f}}. \end{cases} \tag{17}$$

Topsis method [87,88] is applied to obtain the final optimal

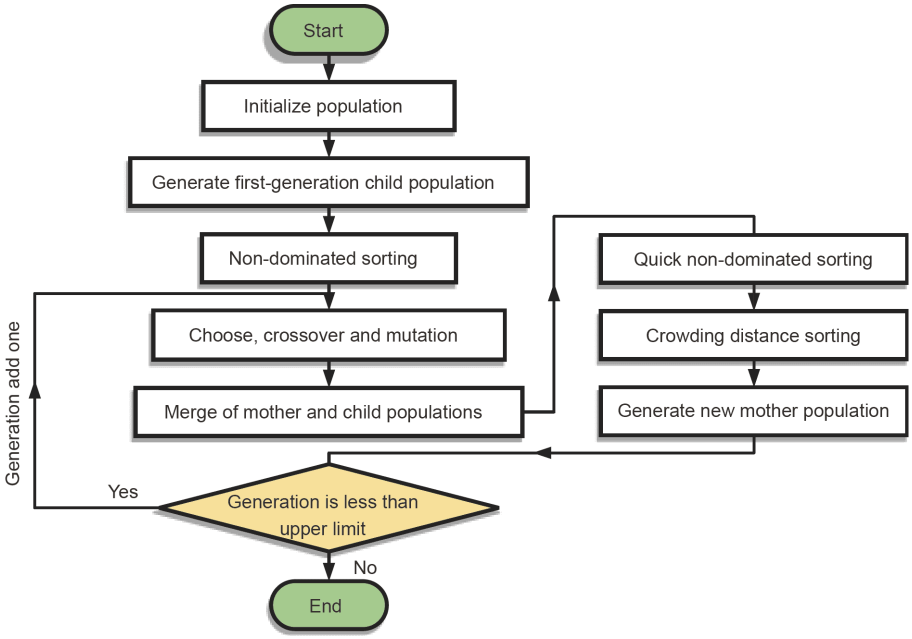

Figure 18 (Color online) Flowchart with application of NSGA-II algorithm.

solution, which is based on the distance away from the pros and cons. The weighted coefficient of each attribute can be flexibly selected according to diversified backgrounds, and then one can obtain the values of corresponding sub-objectives, respectively. For instance, as the dimensionless diameter of cooling channels is optimized which is in concord with the results of Sect. 3.1, Figure 19 shows the scatter diagram of ΔT versus $\dot{W}$ at p=9 and ϕ=0.05. The weighted coefficients of these two sub-objectives are presumed to be 0.5 and 0.5, respectively. As a result, the optimal geometry of the NUHG radial-pattern disc is yielded by applying Topsis method to proceed with multi-attribute decision, i.e., $\tilde{d}_{\text{opt}}$=0.10 along with ΔT=33.8 K and $\dot{W}$=2.29×10^{-5} W. It is proven that the result derived of Topsis decision is consistent with that of linear weighted method, and by this means the credibility of Topsis decision and linear weighted method are verified by each other.

On the basis of NSGA-II algorithm compiled by Matlab, Livelink with Matlab is integratedly invoked to run the aforementioned three-dimensional thermo-fluid model established in the software of COMSOL Multiphysics. Upon this, NSGA-II algorithm should be initialized. Herein, the number of population is 50, the probability of crossover is 0.9, and the probability of mutation is 0.1. After 30 generations of evolution, the Pareto optimal solution set of the MOOP is procured as shown in Figure 20. It is found that at the same cost of pumping power, the MTD in the dendritic-pattern disc decreases with the increase of the NUHG coefficient. This manifests that loading the heat source as close to the cooling water inlet as possible is propitious to reduce the MTD and in the meantime promotes the overall thermal and flow performance at the same cost of pumping power. From exertion of multi-attribute decision, the optimal solution with weighted coefficients of 0.5 and 0.5 is determined. In the case of p=0, the optimal constructs are $\tilde{d}_{\text{opt}}$=0.0184, α_{opt}=0.806 and β_{opt}=0.800, while the corresponding sub-objectives are ΔT=27.2 K and $\dot{W}$=4.05×10^{-5} W. In the case of p=9, the optimal constructs are $\tilde{d}_{\text{opt}}$=0.0773, α_{opt}=0.603 and β_{opt}=0.849, while the corresponding sub-objectives are ΔT=25.8 K and $\dot{W}$=3.77×10^{-5} W, respectively. As the NUHG coefficient is increased from 0 to 9, the MTD is decreased by 5.1%, and the pumping power is decreased by 6.9%. Furthermore, Figure 21 presents the temperature contours of the optimal dendritic-pattern disc in the case that the weighted coefficient is equal to 0.5. Table 7 shows the effects of p on the optimal constructs and performance indexes of the first order dendritic-pattern disc under different heat generating conditions. As shown in Table 7, one can see that as p increases, the optimal length coefficient (α_{opt}) gradually decreases, while the optimal angle coefficient (β_{opt}) first increases and then decreases.

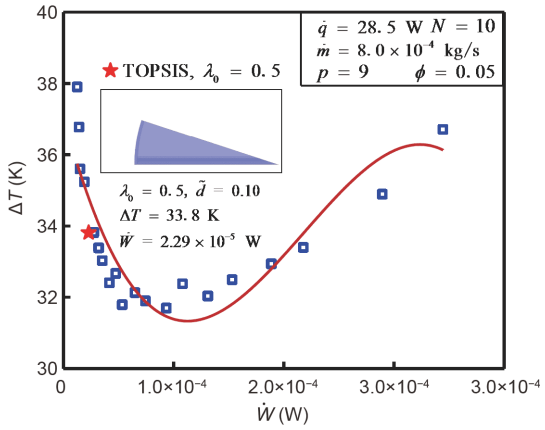

Figure 19 (Color online) Scatter diagram of ΔT versus $\dot{W}$ and Topsis decision verification.

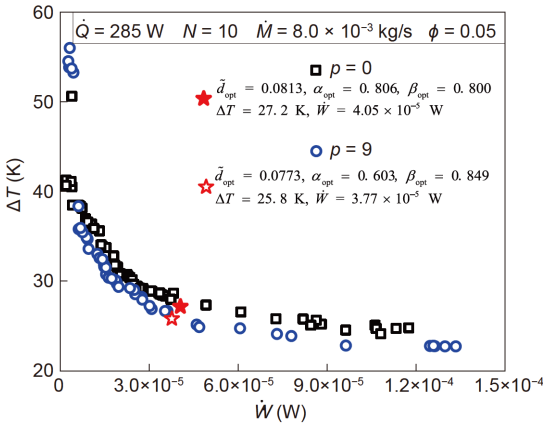

Figure 20 (Color online) Pareto optimal sets under different heat generating conditions.

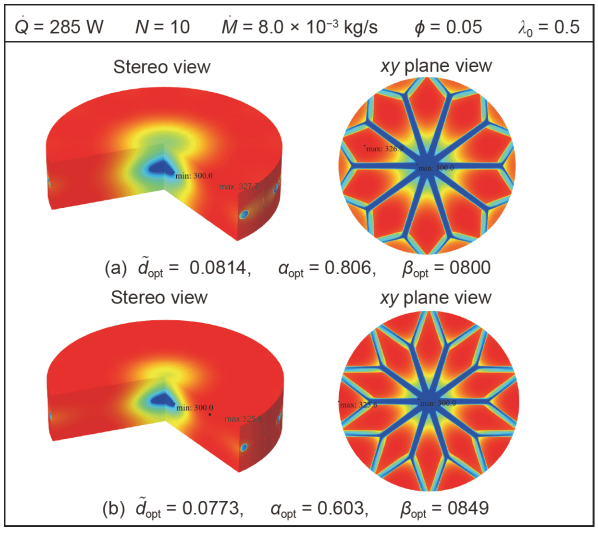

Figure 21 (Color online) Comparison of the optimal geometries of the dendritic-pattern disc. (a) p=0; (b) p=9.

As shown in Figure 8, the sub-objectives of the optimal solution for the radial-pattern disc with only one degree-of-

Table 7 Effects of p on the optimal constructs and performance indexes of the first order dendritic-pattern disc under different heat generating conditions

NUHG coefficient	$\tilde{d}_{opt}$	α_{opt}	β_{opt}	ΔT (K)	$\dot{W}$ (W)
p=0	0.0814	0.806	0.800	27.2	4.05×10^{-5}
p=3	0.0846	0.755	0.847	27.0	3.64×10^{-5}
p=6	0.0801	0.656	0.876	26.2	3.84×10^{-5}
p=9	0.0773	0.603	0.849	25.8	3.77×10^{-5}

freedom are computed to be ΔT=33.8 K and $\dot{W}$=2.29×10^{-5} W, respectively. As shown in Figure 16, the sub-objectives of the optimal solution for the dendritic-pattern disc with two degrees-of-freedom are computed to be ΔT =27.5 K and $\dot{W}$=3.66×10^{-5} W, respectively. As shown in Figure 21, the sub-objectives of the optimal solution for the dendritic-pattern disc with three degrees-of-freedom are ΔT =27.8 K and $\dot{W}$=3.77×10^{-5} W, respectively. When optimized with two degrees-of-freedom, the MTD is reduced by 18.6% compared with the counterpart from single degree-of-freedom optimization, while the pumping power is increased by 59.8%. When optimized with three degrees-of-freedom, the MTD is decreased by 6.2% compared with the counterpart from two degrees-of-freedom optimization, while the pumping power is increased by 3.0%. Apparently, it is indicated that as two sub-objectives contradict against each other, the improvement of one sub-objective will inevitably elicit the deterioration of the alternative. The engineering designers need to implement the constructal design for a NUHG disc in view of practical needs, so as to procure the optimal heat transfer performance under the premise of a lower pumping power.

5 Conclusions

After a view to the phenomenon of NUHG among electronic devices, this paper establishes a three-dimensional disc model with NUHG for heat dissipation problem. In its interior, the radial- and dendritic-pattern cooling channels are equidistantly strewn over the body to realize enhanced convection. From exertion of constructal design method and finite element method, the radial- and dendritic-pattern discs are stepwise optimized with design variables as the diameter, length ratio and angle ratio of the cooling channels. These foregoing variables are exploited as three degrees-of-freedom which are free to morph. The total heat generating rate and volume ratio of cooling channels over the entire disc are set as the two constraints. First, a composite objective function that takes the MTD and pumping power into account is applied as an optimization objective. Then, NSGA-II algorithm is invoked to optimize the multi-objective optimization problem and further yield the Pareto optimal solution set. Upon this, Topsis method is used to determine the final solutions under given weighted coefficients. The results reveal that follows.

(1) More heating components or devices should be installed as close to the inlet of cooling water as possible, which is propitious to reduce the hot spot temperature at the same cost of pumping power. Thus, this improves the real-time operating performance and prolongs the service life-span.

(2) As the weighted coefficients dictating two sub-objectives are 0.5 and 0.5, respectively, the optimal constructs of the radial-pattern disc obtained from Topsis decision are in good agreements with the counterparts obtained from linear weighted method, and by this means the credibilities of Topsis decision and linear weighted method are verified by each other.

(3) When optimized with two degrees-of-freedom, the MTD is reduced by 18.6% compared with that obtained from single degree-of-freedom optimization, while the pumping power is increased by 59.8%. When optimized with three degrees-of-freedom, the MTD is decreased by 6.2% compared with the counterpart from two degrees-of-freedom optimization, while the pumping power is increased by 3.0%.

(4) As the two considered sub-objectives form a game against each other, it is requisite to take not only the extreme temperature that electronic components can bear, but also the pumping power needed to sustain fluid flow into account. One should not emphasize on one sub-objective at the expense of the other, but should procure the optimal trade-off between heat transfer and fluid flow.

The outcomes obtained in this paper can contribute to the design of practical electronic packages like PCB and individual electronic components to a promising thermo-fluid performance. In the following research, one can insert arrays of fins into the cooling channel in order to harvest a better thermo-fluid performance.

This work was supported by the National Natural Science Foundation of China (Grant Nos. 51779262 and 51579244), and the Independent Project of Naval University of Engineering (Grant No. 425317Q017).

1 Sohel Murshed S M, Nieto de Castro C A. A critical review of traditional and emerging techniques and fluids for electronics cooling. Renew Sustain Energy Rev, 2017, 78: 821–833
2 Tuckerman D B, Pease R F W. High-performance heat sinking for VLSI. IEEE Electron Device Lett, 1981, 2: 126–129
3 Xie X L, Liu Z J, He Y L, et al. Numerical study of laminar heat

transfer and pressure drop characteristics in a water-cooled mini-channel heat sink. Appl Thermal Eng, 2009, 29: 64–74
4 Bejan A. Street network theory of organization in nature. J Adv Transp, 1996, 30: 85–107
5 Bejan A. Constructal-theory network of conducting paths for cooling a heat generating volume. Int J Heat Mass Transfer, 1997, 40: 799–816
6 Bejan A. Shape and Structure, from Engineering to Nature. Cambridge: Cambridge University Press, 2000
7 Bejan A, Lorente S. Design with Constructal Theory. Hoboken: Wiley, 2008
8 Lorenzini G, Moretti S, Conti A. Fin Shape Thermal Optimization Using Bejan's Constructal Theory. San Francisco: Morgan & Claypool Publishers, 2011
9 Chen L G. Progress in study on constructal theory and its applications. Sci China Tech Sci, 2012, 55: 802–820
10 Bejan A. Constructal law: Optimization as design evolution. J Heat Transfer, 2015, 137: 061003
11 Chen L G, Feng H J. Multi-objective Constructal Optimizations for Fluid Flow, Heat and Mass Transfer Processes (in Chinese). Beijing: Science Press, 2016
12 Hajmohammadi M R. Introducing a ψ-shaped cavity for cooling a heat generating medium. Int J Thermal Sci, 2017, 121: 204–212
13 Feng H J, Chen L G, Xie Z H. Multi-disciplinary, multi-objective and multi-scale constructal optimizations for heat and mass transfer processes performed in Naval University of Engineering, a review. Int J Heat Mass Transfer, 2017, 115: 86–98
14 Rocha L A O, Lorente S, Bejan A. Constructal theory in heat transfer. In: Handbook of Thermal Science and Engineering. New York: Springer, 2018. 329–360
15 Miguel A F, Rocha L A O. Tree-Shaped Fluid Flow and Heat Transfer. New York: Springer, 2018
16 Chen L G, Feng H J, Xie Z H, et al. Progress of constructal theory in China over the past decade. Int J Heat Mass Transfer, 2019, 130: 393–419
17 Lorente S, Bejan A. Current trends in constructal law and evolutionary design. Heat Trans Asian Res, 2019, 48: 3574–3589
18 Bejan A. Freedom and Evolution: Hierarchy in Nature, Society and Science. Cham: Springer, 2020
19 Yang A B, Chen L G, Xie Z H, et al. Constructal heat transfer rate maximization for cylindrical pin-fin heat sinks. Appl Thermal Eng, 2016, 108: 427–435
20 Lu Z, Zhang K, Liu J, et al. Effect of branching level on the performance of constructal theory based Y-shaped liquid cooling heat sink. Appl Thermal Eng, 2020, 168: 114824
21 Chen L G, Yang A B, Feng H J, et al. Constructal design progress for eight types of heat sinks. Sci China Tech Sci, 2020, 63: 879–911
22 Hajmohammadi M R, Mohammadifar M, Ahmadian-Elmi M. Optimal placement and sizing of heat sink attachments on a heat-generating piece for minimization of peak temperature. ThermoChim Acta, 2020, 689: 178645
23 Wang L, Xie Z H, Chen L G, et al. Equivalent thermal resistance minimization for a circular disc heat sink with reverting microchannels based on constructal theory and entransy theory. Sci China Tech Sci, 2021, 64: 111–121
24 Gong S W, Chen L G, Xie Z H, et al. Constructal optimization of cylindrical heat sources with forced convection based on entransy dissipation rate minimization. Sci China Tech Sci, 2016, 59: 631–639
25 Zhou S B, Chen L G, Sun F R. Constructal optimization for a solid-gas reactor based on triangular element. Sci China Ser E-Tech Sci, 2008, 51: 1554–1562
26 Feng H, Chen L, Xie Z, et al. "Disc-point" heat and mass transfer constructal optimization for solid-gas reactors based on entropy generation minimization. Energy, 2015, 83: 431–437
27 Feng H, Chen L, Xie Z, et al. Generalized constructal optimization for solidification heat transfer process of slab continuous casting based on heat loss rate. Energy, 2014, 66: 991–998
28 Feng H J, Chen L G, Xie Z H, et al. Generalized constructal optimization for the secondary cooling process of slab continuous casting based on entransy theory. Sci China Tech Sci, 2014, 57: 784–795
29 Feng H J, Chen L G, Liu X, et al. Generalized constructal optimization of strip laminar cooling process based on entransy theory. Sci China Tech Sci, 2016, 59: 1687–1695
30 Liu X, Feng H J, Chen L G, et al. Hot metal yield optimization of a blast furnace based on constructal theory. Energy, 2016, 104: 33–41
31 Liu X, Chen L G, Feng H J, et al. Constructal design for blast furnace wall based on the entransy theory. Appl Thermal Eng, 2016, 100: 798–804
32 Liu X, Chen L G, Feng H J, et al. Constructal design of a blast furnace iron-making process based on multi-objective optimization. Energy, 2016, 109: 137–151
33 Chen L G, Liu X, Feng H J, et al. Molten steel yield optimization of a converter based on constructal theory. Sci China Tech Sci, 2018, 61: 496–505
34 Feng H J, Chen L G, Liu X, et al. Constructal optimization of a sinter cooling process based on exergy output maximization. Appl Thermal Eng, 2016, 96: 161–166
35 Feng H J, Chen L G, Xie Z H, et al. Thermal insulation constructal optimization for steel rolling reheating furnace wall based on entransy dissipation extremum principle. Sci China Tech Sci, 2012, 55: 3322–3333
36 Feng H J, Chen L G, Xie Z H, et al. Constructal designs for insulation layers of steel rolling reheating furnace wall with convective and radiative boundary conditions. Appl Thermal Eng, 2016, 100: 925–931
37 Feng H J, Chen L G, Xie Z H, et al. Constructal design for X-shaped hot water network over a rectangular area. Appl Thermal Eng, 2015, 87: 760–767
38 Feng H J, Chen L G, Xie Z H, et al. Constructal design for gas-turbine blade based on minimization of maximum thermal resistance. Appl Thermal Eng, 2015, 90: 792–797
39 Feng H J, Chen L G, Xie Z H, et al. Constructal optimization for H-shaped multi-scale heat exchanger based on entransy theory. Sci China Tech Sci, 2013, 56: 299–307
40 Chen L, Feng H, Xie Z, et al. Thermal efficiency maximization for H- and X-shaped heat exchangers based on constructal theory. Appl Thermal Eng, 2015, 91: 456–462
41 Hajabdollahi H. Multi-objective optimization of plate fin heat exchanger using constructal theory. Int Commun Heat Mass Transfer, 2019, 108: 104283
42 Feng H, Chen L, Wu Z, et al. Constructal design of a shell-and-tube heat exchanger for organic fluid evaporation process. Int J Heat Mass Transfer, 2019, 131: 750–756
43 Feng H J, Xie Z H, Chen L G, et al. Constructal design for supercharged boiler superheater. Energy, 2020, 191: 116484
44 Feng H J, Chen L G, Sun F R. Constructal entransy dissipation rate minimization for leaf-like fins. Sci China Tech Sci, 2012, 55: 515–526
45 Feng H J, Chen L G, Xie Z H, et al. Constructal entransy dissipation rate minimization for helm-shaped fin with inner heat sources. Sci China Tech Sci, 2015, 58: 1084–1090
46 Das R, Kundu B. Forward and inverse nonlinear heat transfer analysis for optimization of a constructal T-shape fin under dry and wet conditions. Int J Heat Mass Transfer, 2019, 137: 461–475
47 Hajmohammadi M R, Ahmadian M, Nourazar S S. Introducing highly conductive materials into a fin for heat transfer enhancement. Int J Mech Sci, 2019, 150: 420–426
48 Hazarika S A, Deshmukhya T, Bhanja D, et al. A novel optimum constructal fork-shaped fin array design for simultaneous heat and mass transfer application in a space-constrained situation. Int J Thermal Sci, 2020, 150: 106225
49 Hajmohammadi M R, Gholamrezaie S, Ahmadpour A, et al. Effects of applying uniform and non-uniform external magnetic fields on the optimal design of microchannel heat sinks. Int J Mech Sci, 2020, 186: 105886
50 Hajmohammadi M R, Rasouli E, Ahmadian Elmi M. Geometric optimization of a highly conductive insert intruding an annular fin. Int J

Heat Mass Transfer, 2020, 146: 118910
51 Feng H J, Chen L G, Xie Z H. Constructal entransy dissipation rate minimization for X-shaped vascular networks. Sci China Tech Sci, 2019, 62: 2195–2203
52 Wu Z X, Feng H J, Chen L G, et al. Optimal design of dual-pressure turbine in OTEC system based on constructal theory. Energy Convers Manage, 2019, 201: 112179
53 Joshi V, Rathod M K. Constructal enhancement of thermal transport in latent heat storage systems assisted with fins. Int J Thermal Sci, 2019, 145: 105984
54 Wu Z X, Feng H J, Chen L G, et al. Pumping power minimization of an evaporator in ocean thermal energy conversion system based on constructal theory. Energy, 2019, 181: 974–984
55 Wu Z X, Feng H J, Chen L G, et al. Constructal thermodynamic optimization for ocean thermal energy conversion system with dual-pressure organic Rankine cycle. Energy Convers Manage, 2020, 210: 112727
56 Wechsatol W, Lorente S, Bejan A. Optimal tree-shaped networks for fluid flow in a disc-shaped body. Int J Heat Mass Transfer, 2002, 45: 4911–4924
57 Lorente S, Wechsatol W, Bejan A. Optimization of tree-shaped flow distribution structures over a disc-shaped area. Int J Energy Res, 2003, 27: 715–723
58 Wechsatol W, Lorente S, Bejan A. Tree-shaped flow structures: are both thermal-resistance and flow-resistance minimisations necessary? Int J Exergy, 2004, 1: 2–17
59 Reddy B V K, Ramana P V, Narasimhan A. Steady and transient thermo-hydraulic performance of disc with tree-shaped micro-channel networks with and without radial inclination. Int J Thermal Sci, 2008, 47: 1482–1489
60 Revellin R, Thome J R, Bejan A, et al. Constructal tree-shaped microchannel networks for maximizing the saturated critical heat flux. Int J Thermal Sci, 2009, 48: 342–352
61 Daguenet-Frick X, Bonjour J, Revellin R. Constructal microchannel network for flow boiling in a disc-shaped body. IEEE Trans Comp Packag Technol, 2010, 33: 115–126
62 Ghaedamini H, Salimpour M R, Campo A. Constructal design of reverting microchannels for convective cooling of a circular disc. Int J Thermal Sci, 2011, 50: 1051–1061
63 Feng H, Chen L, Xie Z, et al. Constructal optimization of a disc-shaped body with cooling channels for specified power pumping. Int J Low-Carbon Tech, 2015, 10: 229–237
64 Salimpour M R, Menbari A. Analytical optimization of constructal channels used for cooling a ring shaped body based on minimum flow and thermal resistances. Energy, 2015, 81: 645–651
65 Bejan A, Errera M R. Convective trees of fluid channels for volumetric cooling. Int J Heat Mass Transfer, 2000, 43: 3105–3118
66 Bello-Ochende T, Liebenberg L, Meyer J P. Constructal cooling channels for micro-channel heat sinks. Int J Heat Mass Transfer, 2007, 50: 4141–4150
67 Xiao Q H, Chen L G, Sun F R. Constructal entransy dissipation rate and flow-resistance minimizations for cooling channels. Sci China Techl Sci, 2010, 53: 2458–2468
68 Zhang C, Chen Y, Wu R, et al. Flow boiling in constructal tree-shaped minichannel network. Int J Heat Mass Transfer, 2011, 54: 202–209
69 Olakoyejo O T, Bello-Ochende T, Meyer J P. Constructal conjugate cooling channels with internal heat generation. Int J Heat Mass Transfer, 2012, 55: 4385–4396
70 Xie G, Asadi M, Sunden B, et al. Constructal theory based geometric optimization of wavy channels in the low Reynolds number regime. J Electron Packaging, 2014, 136: 031013
71 Farzaneh M, Salimpour M R, Tavakoli M R. Design of bifurcating microchannels with/without loops for cooling of square-shaped electronic components. Appl Thermal Eng, 2016, 108: 581–595
72 Yang A B. Performance analyses and multi-objective constructal optimizations for four kinds of heat sinks (in Chinese). Dissertation for Doctoral Degree. Wuhan: Naval University of Engineering, 2017
73 Feijó B C, Lorenzini G, Isoldi L A, et al. Constructal design of forced convective flows in channels with two alternated rectangular heated bodies. Int J Heat Mass Transfer, 2018, 125: 710–721
74 Samal B, Barik A K, Awad M M. Thermo-fluid and entropy generation analysis of newly designed loops for constructal cooling of a square plate. Appl Thermal Eng, 2019, 156: 250–262
75 Khalifa M A, Jaffal H M. Effects of channel configuration on hydrothermal performance of the cylindrical mini-channel heat sinks. Appl Thermal Eng, 2019, 148: 1107–1130
76 Lugarini A, Franco A T, Errera M R. Flow distribution uniformity in a comb-like microchannel network. Microfluid Nanofluid, 2019, 23: 44
77 You J, Feng H, Chen L, et al. Constructal design and experimental validation of a non-uniform heat generating body with rectangular cross-section and parallel circular cooling channels. Int J Heat Mass Transfer, 2020, 148: 119028
78 Feng H, Chen L, Xie Z, et al. Constructal design for a rectangular body with nonuniform heat generation. Eur Phys J Plus, 2016, 131: 274
79 Feng H J, Chen L G, Xie Z H, et al. Constructal entransy dissipation rate minimization of a rectangular body with nonuniform heat generation. Sci China Tech Sci, 2016, 59: 1352–1359
80 You J, Feng H, Chen L, et al. Constructal optimization for cooling a non-uniform heat generating radial-pattern disc by conduction. Entropy, 2018, 20: 685
81 Konan H C, Cetkin E. Snowflake shaped high-conductivity inserts for heat transfer enhancement. Int J Heat Mass Transfer, 2018, 127: 473–482
82 You J, Feng H, Chen L, et al. Heat conduction constructal optimization for nonuniform heat generating area based on triangular element. Int J Heat Mass Transfer, 2018, 117: 896–902
83 Chen L, You J, Feng H, et al. Constructal optimization for “disc-point” heat conduction with nonuniform heat generating. Int J Heat Mass Transfer, 2019, 134: 1191–1198
84 You J, Feng H, Chen L, et al. Constructal design of nonuniform heat generating area based on triangular elements: A case of entropy generation minimization. Int J Thermal Sci, 2019, 139: 403–412
85 Razera A L, da Fonseca R J C, Isoldi L A, et al. Constructal design of a semi-elliptical fin inserted in a lid-driven square cavity with mixed convection. Int J Heat Mass Transfer, 2018, 126: 81–94
86 Cetkin E, Oliani A. The natural emergence of asymmetric tree-shaped pathways for cooling of a non-uniformly heated domain. J Appl Phys, 2015, 118: 024902
87 Ge Y, Wang S, Liu Z, et al. Optimal shape design of a minichannel heat sink applying multi-objective optimization algorithm and three-dimensional numerical method. Appl Thermal Eng, 2019, 148: 120–128
88 Tang C Q, Feng H J, Chen L G, et al. Power density analysis and multi-objective optimization for a modified endoreversible simple closed Brayton cycle with one isothermal heating process. Energy Rep, 2020, 6: 1648–1657
89 Zhang L, Chen L G, Xia S J, et al. Multi-objective optimization for helium-heated reverse water gas shift reactor by using NSGA-II. Int J Heat Mass Transfer, 2020, 148: 119025
90 Wu Z X, Feng H J, Chen L G, et al. Performance optimization of a condenser in ocean thermal energy conversion (otec) system based on constructal theory and a multi-objective genetic algorithm. Entropy, 2020, 22: 641